



Research article

Structural, thermoelectric, and magnetic properties of pure and Ti-doped $\text{Ca}_3\text{Co}_4\text{O}_9$ ceramic compounds

Cihat Boyraz^{*1} ¹ Marmara University, Faculty of Technology, Department of Mechanical Engineering, 34854, Istanbul, Türkiye

Abstract

The effect of the Ti element on the incommensurately layered thermoelectric oxide material $\text{Ca}_3\text{Co}_4\text{O}_9$ is investigated. This study compares the structural, morphological, thermoelectric, and magnetic properties of $\text{Ca}_3(\text{Co}_{3.7}\text{Ti}_{0.3})\text{O}_9$ composition to the pristine $\text{Ca}_3\text{Co}_4\text{O}_9$. No significant enhancement of the Seebeck coefficient compared to $\text{Ca}_3\text{Co}_4\text{O}_9$ is observed in the Ti-doped sample. The magnetic properties of the pristine and Ti-doped $\text{Ca}_3\text{Co}_4\text{O}_9$ are detailed, and the possible correlations between pristine and Ti-doped $\text{Ca}_3\text{Co}_4\text{O}_9$ are established. In M-H measurements, the effect of Ti in low temperatures revealed a magnetic phase transition due to two sublattices exhibiting wavy behavior. For each sample, magnetic inhomogeneity in the long-range ferromagnetic ordering, which is clear almost before 19 K, is observed through FC and ZFC curves. The findings on the physical properties of both samples are discussed, considering the previously published results.

Keywords: Structural and magnetic properties; thermoelectricity; Ti-doped $\text{Ca}_3\text{Co}_4\text{O}_9$

1. Introduction

More The reduction of natural energy sources and the high demand for these resources make it crucial to develop new and alternative energy sources. For example, converting waste heat directly into electricity is an economical, environmentally friendly, efficient alternative. Moreover, materials with thermoelectric properties, like double-stranded DNA, are used in life sciences and various biotechnological applications (Yueqi et al., 2016; Heussman et al., 2022; Mogheiseh et al., 2023). The molecular resistance has a linear relationship with length due to the thermoelectric effect in both the tunneling and hopping regimes, in which electrons or holes move sequentially along molecules from one end to the other through many steps in biology (Yueqi et al., 2016; Kun et al., 2019; Li et al., 2019; Chen et al., 2021; Seif et al., 2021).

Studying the thermoelectric effect in single molecules can be used for various purposes, including evaluating the alignment of the molecular orbitals, comprehending the energy conversion

mechanism connected to charge transport, and figuring out whether electrons or holes are responsible for charge transport. Thermoelectric (TE) devices which are low-cost, pollution and maintenance-free, allow for the harvest of waste energy. Various sources such as gasoline-fueled internal combustion engines, power generators (the Seebeck effect), and coolers (the Peltier effect) (Ohtaki et al., 1996; Zang et al., 2020; Ruan et al., 2021; Amaveda et al., 2022) are presently available. But to be efficient, TE devices need to exhibit stable high thermal and chemical properties at elevated temperatures in the air. For practical industrial purposes, thermoelectric materials' performance and relative utility can be evaluated by the figure of merit ZT which is required to be >1 . So far, some oxide systems have been investigated, such as $(\text{Zn}, \text{Al}) \text{O}$ (Ohtaki et al., 1996), La_2CuO_4 (Liu et al., 2022), and In_2O_3 (Klich et al., 2021).

Recently studies at ambient temperature for nano-structured Bi_2Te_3 - Bi_2Se_3 superlattices have yielded a promising high TE figure of merit $Z_T > 2$ (Ozkendir et al., 2022). However, the effectiveness of these systems is incomparable, even with

* Corresponding author.

E-mail address: cboyraz@marmara.edu.tr (C. Boyraz).<https://doi.org/10.51753/flsrt.1249167> Author contributions

Received 08 February 2023; Accepted 11 July 2023

Available online 26 August 2023

2718-062X © 2023 This is an open access article published by Dergipark under the [CC BY](https://creativecommons.org/licenses/by/4.0/) license.

alloys and semiconductors. Even if the popularity of the ongoing research on TE devices has tended to quantum dots or nanowires, such systems are both toxic and unstable at high temperatures. Oxide materials such as NaCo_2O_4 (Perac et al., 2022) and $\text{Ca}_3\text{Co}_4\text{O}_9$ (Klie et al., 2012) have been revealed to possess high thermoelectric properties, which are still not well understood and probably related to the correlation between the behavior of the electrons and phonons in anisotropic phase environments and the low dimensionality of the crystal structure. However, due to the distribution of grains' random orientation in the ceramics, polycrystalline $\text{Ca}_3\text{Co}_4\text{O}_9$ shows a relatively low figure of merit (grain boundary scattering leading to enhanced electrical resistivity). Therefore, the homogeneity of composition during the ceramic sintering process controlling grain growth and different dopants' effects are essential to improve this figure of merit.

Among the layered oxides, increasing attention has been given to $\text{Ca}_3\text{Co}_4\text{O}_9$ as one of the most promising thermoelectric materials (Shi et al., 2021). The crystal structure of $\text{Ca}_3\text{Co}_4\text{O}_9$ can be viewed as rocksalt-type Ca_2CoO_3 layers with a CdI_2 -like CoO_2 layer stacked (Amaveda et al., 2022). Many dopants have been utilized by choosing different kinds of ions at various ratios to improve and optimize thermoelectric performance (Li et al., 2022). Other atomic substitutions for the Ca-site in the rock-salt type Ca_2CoO_3 layers of $\text{Ca}_3\text{Co}_4\text{O}_9$ revealed a practical enhancement in the Seebeck coefficient and texture (Shi et al., 2021). This improvement should be the reason for an increase in carrier mobility due to the effect of the different sizes of atoms in the $\text{Ca}_3\text{Co}_4\text{O}_9$ system. Pristine and elemental substituted Ca-Co-O systems are expected to exhibit a high Seebeck coefficient by optimizing texture, the control of carrier density, and mobility.

In this study, Ti substituted $\text{Ca}_3\text{Co}_4\text{O}_9$ sample, synthesized by solid-state reaction method to figure out the structural and magnetic effects of Ti atom in the $\text{Ca}_3\text{Co}_4\text{O}_9$ system, was investigated. The enhancement of TE performance, which is related to the induced Co spin-entropy via the Ti doping effect in $[\text{Ca}_2\text{CoO}_3]$ and $[\text{CoO}_2]$ sublayers, was exhibited by revealing the Seebeck coefficients of both $\text{Ca}_3\text{Co}_4\text{O}_9$ and $\text{Ca}_3(\text{Co}_{3.7}\text{Ti}_{0.3})\text{O}_9$. The magnetic effect of Ti ions on the $\text{Ca}_3\text{Co}_4\text{O}_9$ system was demonstrated, and the results were compared by $\text{Ca}_3\text{Co}_4\text{O}_9$ composition.

2. Materials and methods

In this study, the powders were synthesized using a solid-state reaction technique with sub-micrometer particle size and the same (99.9% Stream Chemicals) purity. All samples were prepared from CaCO_3 , Co_3O_4 , and TiO_2 from reagent-grade powders. These powders in specific proportions were weighed to obtain the nominal composition of $\text{Ca}_3(\text{Co}_{3.7}\text{Ti}_{0.3})\text{O}_9$ and $\text{Ca}_3\text{Co}_4\text{O}_9$ separately. In an agate mortar, the stoichiometric mixtures of oxides were homogenized and mixed by a stirrer in an isopropyl alcohol medium ($\text{C}_3\text{H}_8\text{O}$) for five h at 230 rpm. The compound was calcinated at (950°C) for 12-24 h in the air to activate phase transition and form.

The samples were cooled to room temperature and ground to obtain high-quality homogenized mixtures and recalinated at (950°C) for 24 h in air. The weight difference in all cases was negligible. 1000 Mpa uniaxial pressure was applied to the pellets, and after that, the pellets were sintered at 950°C for 24h in an air furnace. The crystalline phase and the oxides were analyzed by θ - 2θ two-circle XRD setup (Bruker AXS D8

Advance) using a Cu $K\alpha$ source. The size of the grains and the elemental compositions of the obtained samples were determined by SEM and an in-situ attachment of EDX with the model of JOEL 7000 FE and INCA (Oxford Instrument) software. As a function of magnetic field and temperature, the static magnetization measurements were conducted by a vibrating Sample Magnetometer. Quantum Design PPMS was equipped with a thermal transport option for the in-plane Seebeck coefficient measurements.

3. Results

3.1. Structural and morphological analysis

Crystal properties were investigated by XRD. Fig. 1 shows the XRD patterns of pure $\text{Ca}_3\text{Co}_4\text{O}_9$ and Co-site Ti-doped $\text{Ca}_3\text{Co}_4\text{O}_9$ powder samples produced under the same conditions. A wide range of sintering temperatures (800-950 °C) was used to test the convenient sintering temperature of $\text{Ca}_3\text{Co}_4\text{O}_9$. The decomposition phase of $\text{Ca}_3\text{Co}_4\text{O}_9$ is $\text{Ca}_3\text{Co}_2\text{O}_6$, of which peaks were marked with the # symbol in Fig. 1. At 950°C sintering temperature, the decomposition reaction rarely occurs. It is known in the literature that at over 1200°C, the decomposition reaction of $\text{Ca}_3\text{Co}_4\text{O}_9$ more extensively yields $\text{Ca}_3\text{Co}_2\text{O}_6$ and CoO peaks (Woermann et al., 1970). When lowering the calcinating and sintering temperatures below 750°C, the intensity deteriorates due to the insufficient crystallization phase (Tongfang et al., 2010).

The effects of Ti doping into the $\text{Ca}_3\text{Co}_4\text{O}_9$ depict no clear evidence about the positional shifts of the peaks. However, as shown in Fig. 1, some extra ignorable peaks reveal due to Ti doping. Cohen's method was used to determine the lattice parameters of both $\text{Ca}_3\text{Co}_4\text{O}_9$ and its Ti-doped form (Sari et al., 2023). One such promising material, $\text{Ca}_3\text{Co}_4\text{O}_9$, is incommensurately composed of rocksalt-type Ca_2CoO_3 layers sandwiched between two hexagonal CdI_2 -like CoO_2 layers. The lattice parameters shared by both subystems are $a = 4.8339 \text{ \AA}$, $c = 10.8436 \text{ \AA}$, and $b_1/b_2 = 1.618$ with $\beta = 98.14^\circ$. The $\text{Ca}_3(\text{Co}_{3.7}\text{Ti}_{0.3})\text{O}_9$ composition has the same structural system with the lattice parameters of $a = 4.8332 \text{ \AA}$, $c = 10.8438 \text{ \AA}$, and $b_1/b_2 = 1.617$.

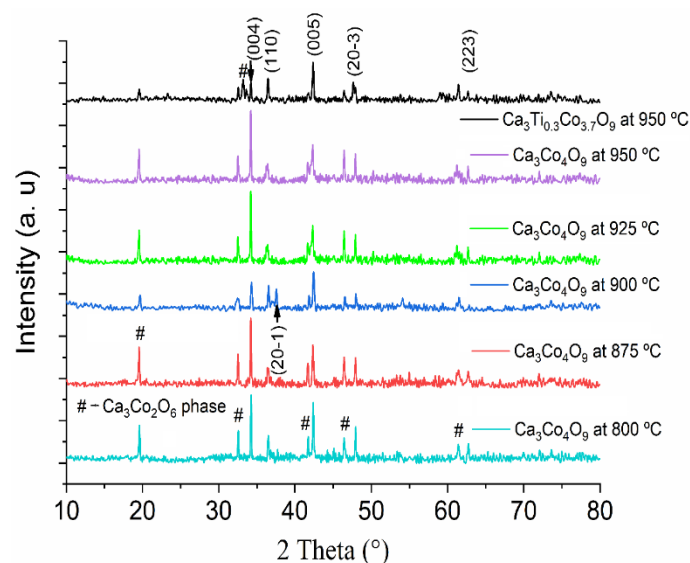


Fig. 1. XRD pattern of $\text{Ca}_3\text{Co}_4\text{O}_9$ at varying annealing temperatures and Ti-doped $\text{Ca}_3\text{Co}_4\text{O}_9$ sample annealed at 950°C are summarized.

The SEM photos of $\text{Ca}_3\text{Co}_4\text{O}_9$ [in (a) and (c)] and $\text{Ca}_3(\text{Co}_{3.7}\text{Ti}_{0.3})\text{O}_9$ [in (b) and (d)] sintered at 950°C for 2 and $5\ \mu\text{m}$ magnifications are shown in Fig. 2. Due to the optimum 950°C (24 h) sintering temperature, porous pellets were minimally formed. This reveals that sintering temperatures below 950°C are insufficient to produce dense $\text{Ca}_3\text{Co}_4\text{O}_9$ and $\text{Ca}_3(\text{Co}_{3.7}\text{Ti}_{0.3})\text{O}_9$ ceramics. A scanning electron microscope study indicated that at high sintering temperature regimes (970 – 1000°C), also many pores were present, and a larger grain size of about $2\ \mu\text{m}$ forms. Over 1000°C sintering temperature, the surface of the grains became even smoother, and grains coarsened (Dos Santos et al., 2020). The observed physical view of the grains should be an indicator of partially melted surface grains (Koshibae et al., 2000; Yang et al., 2009; Dos Santos et al., 2020). The EDX measurement was performed to quantify the elemental composition of the pellet samples. Quantitative texture analysis of the bulk ceramic materials showed only the composition material peaks of $\text{Ca}_3\text{Co}_4\text{O}_9$ and $\text{Ca}_3(\text{Ti}_{0.3}\text{Co}_{3.7})\text{O}_9$. As seen in Table 1 and Table 2, a convenient compositional quantify with the stoichiometry in the EDX analysis was exhibited for $\text{Ca}_3\text{Co}_4\text{O}_9$ and $\text{Ca}_3(\text{Co}_{3.7}\text{Ti}_{0.3})\text{O}_9$ samples.

Table 1

The EDX measurement results of the $\text{Ca}_3\text{Co}_4\text{O}_9$ sample in K shell energies are depicted.

Element	Weight %	Atomic %	Net Int.	Net Int. Error
O K	30.63	54.44	1081.11	0.01
Ca K	23.22	18.57	4376.83	0.01
Co K	46.15	26.99	1690.21	0.01

Table 2

The EDX measurement results of the Ti-doped $\text{Ca}_3\text{Co}_4\text{O}_9$ sample in K shell energy levels are summarized.

Element	Weight %	Atomic %	Net Int.	Net Int. Error
O K	24.78	50.08	566.3	0.01
Ca K	26.47	21.35	1808.31	0.01
Ti K	10.48	5.77	730.04	0.01
Co K	38.27	22.8	630.9	0.01

The Heikes formula (Eq. 1) is useful for determining the Seebeck coefficient in strongly correlated oxide materials (Shi et al., 2021).

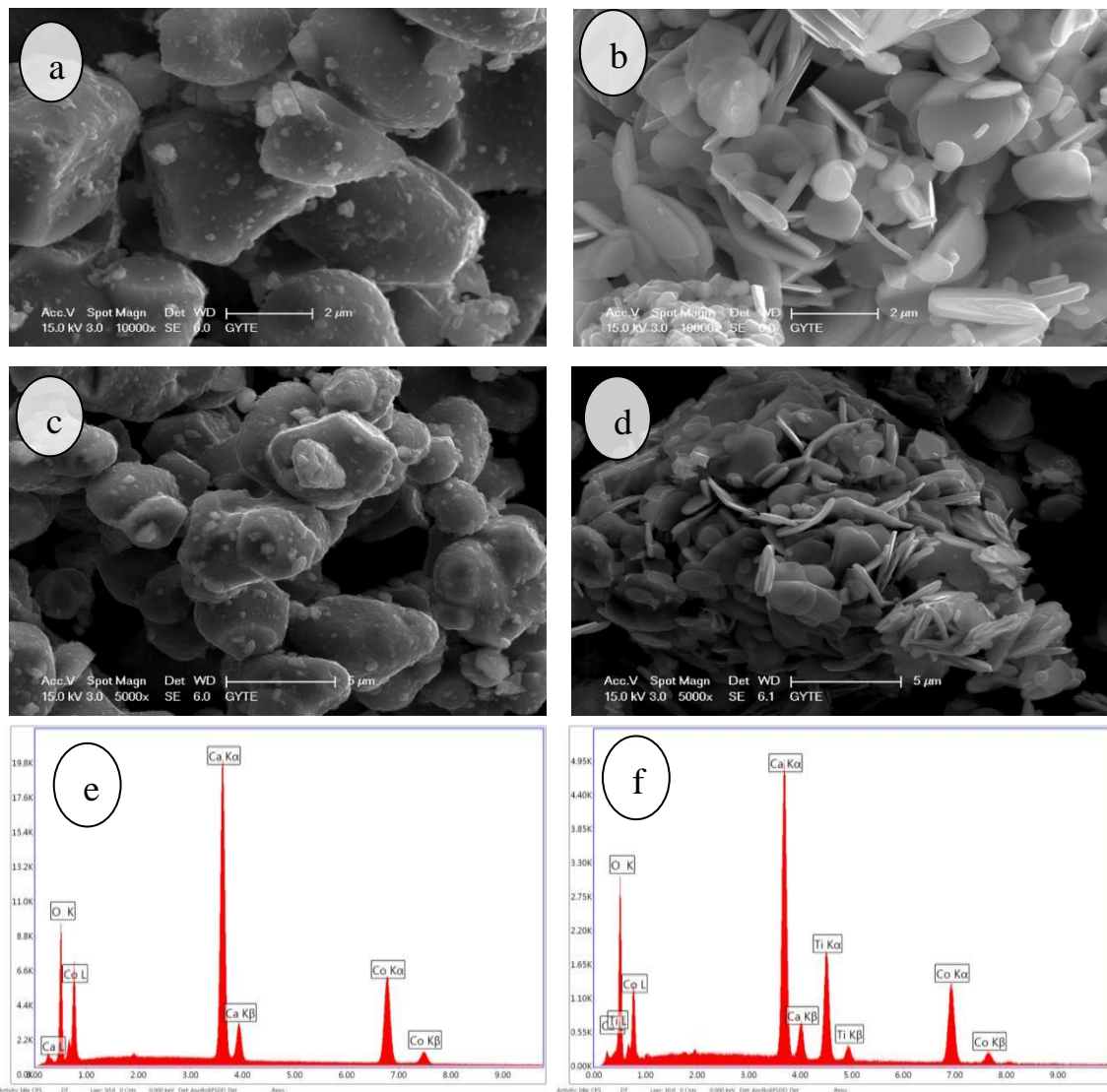


Fig. 2. The SEM images of $\text{Ca}_3\text{Co}_4\text{O}_9$ in (a), (c), and Ti-doped $\text{Ca}_3\text{Co}_4\text{O}_9$ in (b) and (d) both annealed at 950°C are summarized. In (e) and (f), the EDX measurement results are depicted for $\text{Ca}_3\text{Co}_4\text{O}_9$ and Ti-doped $\text{Ca}_3\text{Co}_4\text{O}_9$ samples, respectively.

3.2. Thermoelectric analysis

$$S = -\frac{k_B}{e} \ln\left(\frac{g_3}{g_4} \frac{1-x}{x}\right) \tag{Eq. 1}$$

In Eq. 1, Co^{4+} concentration is shown by x , k_B is the Boltzmann constant, e is the electronic charge, and the orbital degeneracies of Co^{3+} and Co^{4+} in the CoO_2 layer are given by g_3 and g_4 , respectively. In the literature, $x=0.5$ has been found as a critical concentration value of Co^{4+} in the CoO_2 layers, which results in a Co-valence state of + 3.5 (Li et al., 2022). A possibility of this mixed-valence state in the CoO_2 layer is assumed for the large S . At room temperature, the Seebeck coefficients of pristine bulk $\text{Ca}_3\text{Co}_4\text{O}_9$ and Ti-doped $\text{Ca}_3\text{Co}_4\text{O}_9$ were measured to be $S = 130 \mu\text{V}/\text{K}$ and $S = 136 \mu\text{V}/\text{K}$, respectively. Thus, a slight increment in the Seebeck coefficient of Ti-doped $\text{Ca}_3\text{Co}_4\text{O}_9$ was observed within the experimental uncertainty of the transport measurement setup (Hu et al., 2016).

Similar results for the thin-film form of the Ti-doped $\text{Ca}_3\text{Co}_4\text{O}_9$ were found in the literature (Hu et al., 2016). Some nanoparticle systems also exhibit similar thermoelectric behavior, and those are used in life science (Aksu et al., 2022; Boyraz et al., 2022; Chein et al., 2022; Hinterdinget al., 2022; Boyraz et al., 2023).

3.3. Magnetic analysis

Magnetic field-dependent magnetization measurements

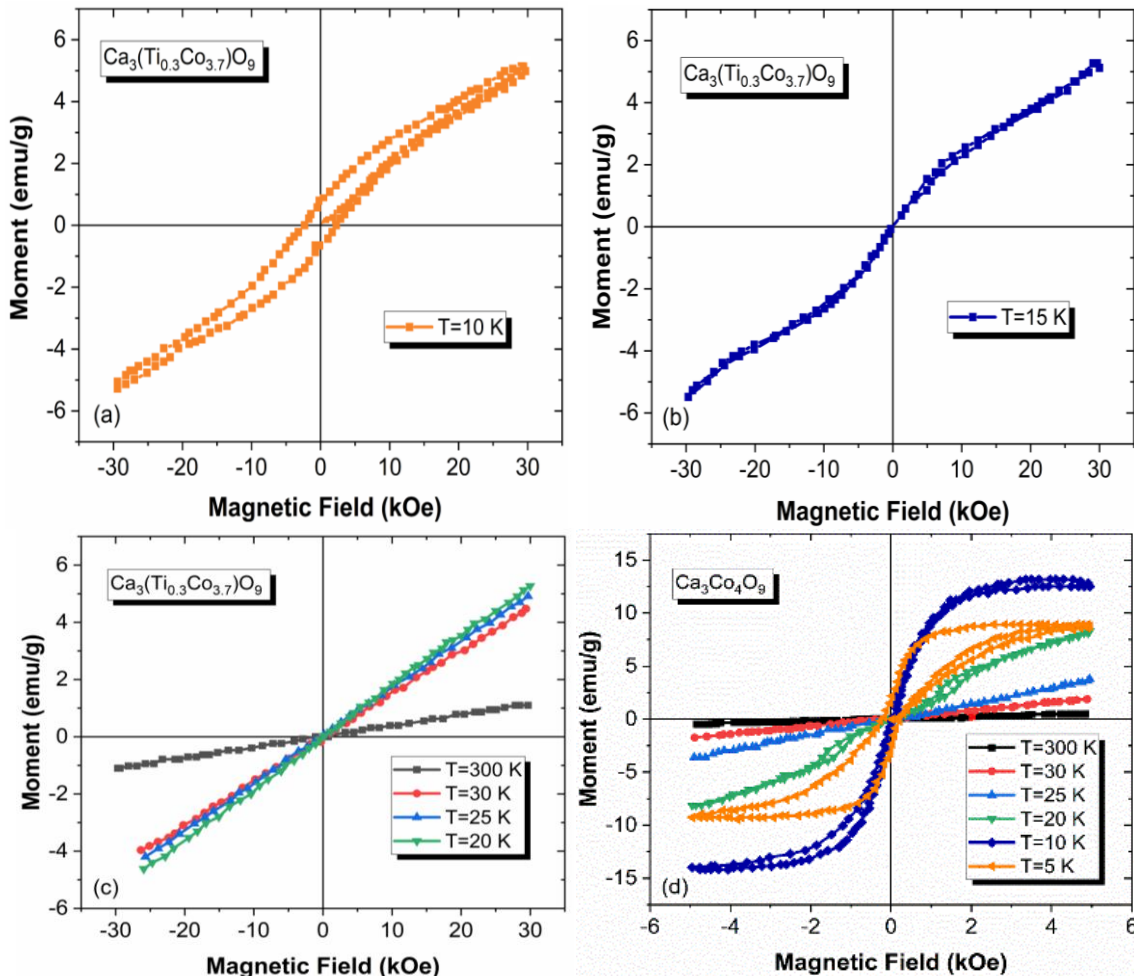


Fig. 3. The magnetic field-dependent magnetization of CTCO in (a), (b), and (c) and CCO in (d) at the given temperatures were exhibited.

conducted for CCO and CTCO samples in a wide temperature range of ($T=5, 10, 20, 25, 30,$ and 300 K) and ($T=10, 15, 20, 25, 30,$ and 300 K) in Fig. 3 respectively. As seen in (a) and (b), the $\text{Ca}_3(\text{Co}_{3.7}\text{Ti}_{0.3})\text{O}_9$ sample exhibits ferromagnetic behavior at 10 and 15 K.

It is known that the crystal structure of $\text{Ca}_3\text{Co}_4\text{O}_9$ can be viewed as rocksalt-type Ca_2CoO_3 layers with CdI_2 -like stacked CoO_2 layer. The wavy behavior in (b) should be the reason for the magnetic phase transition due to two sublattices (Klie et al., 2012). Hence, these two layers provide two sub-lattices with different Curie temperatures (T_c). Similar wavy behavior was observed for CCO at 20 K in Fig. 3 (d). The wavy behavior in low temperatures should not be attributed to the change in the domain structure. Fig. 3 (c) illustrates that $\text{Ca}_3(\text{Co}_{3.7}\text{Ti}_{0.3})\text{O}_9$ and $\text{Ca}_3\text{Co}_4\text{O}_9$ structures show an apparent paramagnetic behavior above 15 K and 20 K, respectively.

Temperature evaluation of magnetization (M) in a field of 50 Oe (FC) and after cooling the sample in ZFC conditions was depicted in Fig. 4 (a) and (b) for the samples $\text{Ca}_3\text{Co}_4\text{O}_9$ and $\text{Ca}_3(\text{Co}_{3.7}\text{Ti}_{0.3})\text{O}_9$ respectively. As seen in Fig. 4 (a) and (b), there is a magnetic phase transition in both $\text{Ca}_3\text{Co}_4\text{O}_9$ (at 20 K) and $\text{Ca}_3(\text{Co}_{3.7}\text{Ti}_{0.3})\text{O}_9$ (at 18.9 K). These magnetic phase transitions have been attributed to the ferr-to-ferromagnetic transitions below Neel temperature. In pristine and Ti-doped CCO, the existence of magnetic inhomogeneity in the long-range ferromagnetic ordering is clear almost before 19 K for each sample due to the separation of each ZFC and FC curve (Hira et al., 2019).

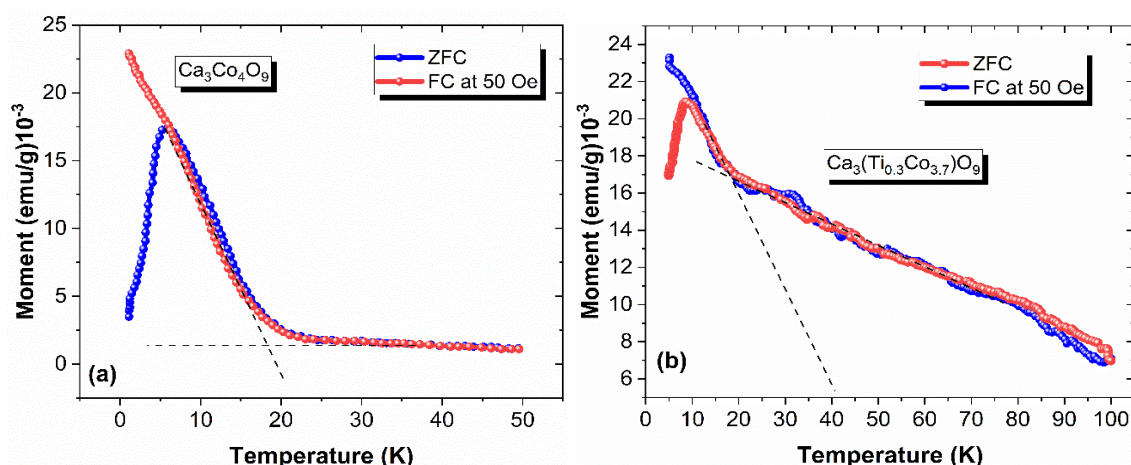


Fig. 4. The temperature-dependent zero-field-cooled (ZFC) and field-cooled (FC) magnetizations for $\text{Ca}_3\text{Co}_4\text{O}_9$ and $\text{Ca}_3(\text{Co}_{3.7}\text{Ti}_{0.3})\text{O}_9$ in (a) and (b) respectively.

4. Conclusion

The pristine and Ti-doped CCO samples were fabricated by the solid-state reaction method. The structural and magnetic characteristics of pure and Ti-doped CCO were compared. The structural effect of Ti in pristine CCO was revealed by calculating lattice parameters indicating a very small variation in the Ti-doped sample. In the literature, the Seebeck coefficient of $\text{Ca}_3\text{Co}_{3.8}\text{Ti}_{0.2}\text{O}_9$ was measured as $S = 135 \mu\text{V}/\text{K}$ which is very close to our measurement result $S = 136 \mu\text{V}/\text{K}$ for $\text{Ca}_3(\text{Co}_{3.7}\text{Ti}_{0.3})\text{O}_9$ (Hu et al., 2016).

In M-H measurements, the effect of Ti in low temperatures revealed itself as a magnetic phase transition due to two sublattices exhibiting wavy behavior.

The separation of each ZFC and FC curve indicates magnetic inhomogeneity in the long-range ferromagnetic ordering, which is clear almost before 19 K for each sample. An increment in the

Seebeck coefficient was observed due to Ti substitution, which also brought inhomogeneity to the pristine CCO. Especially in powder form, the thermoelectric effect provides a new field of study in transport properties in DNA studies. Thus, CCO may be a suitable candidate for molecular studies in life science.

Acknowledgments: This work was supported by the Marmara University BAPKO unit with project number FYL-2022-10334.

Conflict of interest: The author declares that he has no conflict of interests.

Informed consent: The author declares that this manuscript did not involve human or animal participants and informed consent was not collected.

References

- Amaveda, H., Mora, M., Dura, O. J., Torres, M. A., Madre, M. A., Marinel, S., & Sotelo, A. (2022). Influence of ceramic particles additions on the properties of $\text{Ca}_3\text{Co}_4\text{O}_9$. *SN Applied Sciences*, 4(4), 159.
- Boyraz, C., Aksu, P., Guler, A., Arda, L. (2022). The effect of defects formed under pressure on CuCrO_2 delafossite. *SN Applied Sciences*, 4(7), 193.
- Boyraz, C., Aksu, P., Guler, A., Oner, Y., & Fujioka, M. (2023). Short-range magnetic order at low temperatures, exchange bias, and negative magnetization in undoped CuCrO_2 . *Journal of Electronic Materials*, 1-9.
- Boyraz, C., Guler, A., Karatas, O., Aksu, P., Alphan, M. C., & Arda, L. (2022). The investigation of effect of defects on the structural, optical, and magnetic properties of CuAlO_2 . *Acta Physica Polonica A*, 142(4), 464-472.
- Chen, H., & Fraser Stoddart, J. (2021). From molecular to supramolecular electronics. *Nature Reviews Materials*, 6, 804-828.
- Chien, C. W., Chung, L. Y., Subramanian, S., Chia, Y., Chen, T., & Yung, S. F. (2022). Preparation and characterization of CuCrO_2 - CeO_2 nanofibers by electrospinning method. *Journal of Materials Science: Materials in Electronics*, 33, 1091-1100.
- Dos Santos, A. M., Thomazini, D., & Gelfuso, M. V. (2020). Cold sintering and thermoelectric properties of $\text{Ca}_3\text{Co}_4\text{O}_9$ ceramics. *Ceramics International*, 46(9), 14064-14070.
- Heussman, D., Kittell, J., von Hippel, P. H., & Marcus, A. H. (2022). Temperature-dependent local conformations and conformational distributions of cyanine dimer labeled single-stranded-double-stranded DNA junctions by 2D fluorescence spectroscopy. *The Journal of Chemical Physics*, 156(4).
- Hinterding, R., Rieks, D., & Feldhoff, A. (2022). Reaction sintering of $\text{Ca}_3\text{Co}_4\text{O}_9$ with BiCuSeO nanosheets for high-temperature thermoelectric composites. *Journal of Electronic Materials*, 51(2), 532-542.
- Hira, U., Grivel, J. C., Christensen, D. V., Pryds, N., & Sher, F. (2019). Electrical, magnetic and magnetotransport properties of Na and Mo doped $\text{Ca}_3\text{Co}_4\text{O}_9$ materials. *Royal Society of Chemistry Advances*, 9, 31274.
- Hu, X., Phillips, P. J., Mazumdar, D., Carlos, J., Kolesnik, I. S., Gupta, A., Ogut, S., & Klie, R. F. (2016). Atomic and electronic structure of Ti substitution in $\text{Ca}_3\text{Co}_4\text{O}_9$. *Journal of Applied Physics*, 120, 205105.
- Klich, W., & Ohtaki, M. (2021). Thermoelectric properties of Mo-doped bulk In_2O_3 and prediction of its maximum ZT. *Ceramics International*, 47(13), 18116-18121.
- Klie, R. F., Qiao, Q., Paulauskas, T., Gulec, A., Rebola, A., Ogut, S., Prange, M. P., Boyraz, C., Ozdemir, M., Mazumdar, D., & Gupta, A. (2012). Observations of Co^{4+} in a higher spin state and the increase in the seebeck coefficient of thermoelectric $\text{Ca}_3\text{Co}_4\text{O}_9$. *Physical Review Letters*, 108(19), 196601.
- Koshibae, W., Tsutsui, K., & Maekawa, S. (2000). Thermopower in cobalt oxides. *Physical Review B*, 62, 6869.
- Kun, W., Edgar, M., & Pramod, R. (2019). Thermal and thermoelectric properties of molecular junctions. *Advanced Functional Materials*, 30, 1904534.
- Li, Y. N., Wu, P., & Wang, L. (2022). Enhanced thermoelectric properties of $\text{Ca}_3\text{Co}_4\text{O}_9$ by adding nano MoSi_2 . *Ceramics International*, 48(22), 33967-33975.
- Li, Y., Buerkle, M., & Li, G. (2019). Gate controlling of quantum interfe-

- rence and direct observation of anti-resonances in single molecule charge transport. *Nature Materials*, 18, 357-363.
- Liu, S., Qin, B. C., Wang, D. Y., & Zhao, L. D. (2022). Investigations on the thermoelectric transport properties in the hole-doped La_2CuO_4 . *Zeitschrift für Anorganische und Allgemeine Chemie*, 648(15).
- Mogheiseh, M., Etemadi, E., & Hasanzadeh Ghasemi, R. (2023). Design, molecular dynamics simulation, and investigation of the mechanical behavior of DNA origami nanotubes with auxetic and honeycomb structures. *Journal of Biomolecular Structure and Dynamics*, 1-10.
- Ohtaki, M., Ogura, D., Eguchi, K., & Arai, H. (1996). High temperature thermoelectric properties ($\text{Zn}_{1-x}\text{Al}_x$)O. *Journal of Applied Physics*, 79, 1816-1818.
- Ozkendir, O. M., Miyazaki, H., & Gunaydin, S. (2022). Traces of thermoelectric properties on XAFS spectra. *Journal of Electronic Materials*, 51(4), 1740-1751.
- Perac, S., Savic, S. M., Brankovic, Z., Bernik, S., Radojkovic, A., Kojic, S., Vasiljevic, D., & Brankovic, G. (2022). Microstructural, thermoelectric and mechanical properties of Cu substituted NaCo_2O_4 . *Materials*, 15(3), 4470.
- Ruan, C. C., Song, H. Z., & Liu, S. H. (2021). Enhancement of $\text{Ca}_3\text{Co}_4\text{O}_9$ +delta thermoelectric properties by dispersing SiC nanoparticles. *Ceramics International*, 47(5), 6548-6553.
- Sari, Y. W., Tsalsabila, A., Saputra, A., Nuzulia, N. A., & Herbani, Y. (2023). Hydroxyapatite nucleation and growth modulated by amino acid-capped gold nanoparticles: An in vitro study. *Ceramics International*, 49(11), 17166-17173.
- Seif, A., & Yonatan, D. (2021). Spinterface origin for the chirality-induced spin-selectivity effect. *Journal of the American Chemical Society*, 143(35), 14235-14241.
- Shi, Z. M., Cao, S. Y., Araujo, J. M., Zhang, P., Lou, Z. H., Qin, M. J., Xu, J., & Gao, F. (2021). Plate-like $\text{Ca}_3\text{Co}_4\text{O}_9$: A novel lead-free piezoelectric material. *Applied Surface Science*, 536, 1-5.
- Tongfang, Y., Dawei, L., Yun, O., Feiyue, M., Shuhong, X., Li, J. F., & Jiangyu, L. J. (2010). Nanocrystalline thermoelectric $\text{Ca}_3\text{Co}_4\text{O}_9$ ceramics by sol-gel based electrospinning and spark plasma sintering. *The Journal of Physical Chemistry C*, 114, 10061-10065.
- Woermann, E., & Muan, A. (1970). Phase equilibria in the system CaO-Cobalt oxide in air. *Journal of Inorganic and Nuclear Chemistry*, 32, 1455-1459.
- Yang, G., Ramasse, Q., & Klie, R. F. (2009). Direct measurement of Co-ion spin-state transitions in $\text{Ca}_3\text{Co}_4\text{O}_9$ using variable-temperature electron energy-loss spectroscopy. *Applied Physics Letters*, 94, 093112.
- Yueqi, L., Limin, X., Julio, L., Palma, Y. A., & Nongjian, T. (2016). Thermoelectric effect and its dependence on molecular length and sequence in single DNA molecules. *Nature Communications*, 7, 11294.
- Zhang, L., Liu, Y. C., & Li, S. (2020). Thermoelectric performance enhancement by manipulation of Sr/Ti doping in two sublayers of $\text{Ca}_3\text{Co}_4\text{O}_9$. *Journal of Advanced Ceramics*, 9(6), 769-781.

Cite as: Boyraz, C. (2023). Structural, thermoelectric, and magnetic properties of pure and Ti-doped $\text{Ca}_3\text{Co}_4\text{O}_9$ ceramic compounds. *Front Life Sci RT*, 4(2), 79-84.